

Effect of Polymer Topology on Microstructure, Segmental Dynamics, and Ionic Conductivity in PEO/PMMA Based Solid Polymer Electrolytes

Recep Bakar,¹ Saeid Darvishi,² Kunlun Hong,³ Mertcan Han,⁴ Umut Aydemir,^{5,6} Sedat Nizamoglu,^{4,7} and Erkan Senses^{2*}

¹*Department of Material Science and Engineering, Koç University, Sariyer, Istanbul 34450, Turkey*

²*Department of Chemical and Biological Engineering, Koç University, Sariyer, Istanbul 34450, Turkey*

³*Center for Nanophase Materials Sciences, Oak Ridge National Laboratory, Oak Ridge, Tennessee 37831, United States*

⁴*Department of Electrical and Electronics Engineering, Koç University, Sariyer, Istanbul, Turkey*

⁵*Department of Chemistry, Koc University, Sariyer, Istanbul 34450, Turkey*

⁶*Koc University Boron and Advanced Materials Application and Research Center, Sariyer, Istanbul 34450, Turkey*

⁷*Department of Biomedical Science and Engineering, Koç University, Istanbul 34450, Turkey*

KEYWORDS: polymer electrolytes, polymer blends, ionic conductivity, polymer architecture, segmental dynamics

ABSTRACT:

Poly(ethylene oxide) (PEO) based solid polymer electrolytes (SPEs) have attracted much interest due to their high ionic conductivity resulting from inherently fast segmental dynamics and high salt solubility, yet they lack mechanical stability in their neat form. Blending PEO with another rigid, or high glass transition temperature, polymer is a versatile way to improve the mechanical stability; however, the ionic conductivity is strongly reduced due to slower segmental dynamics of highly interpenetrating linear polymer chains. In this work, we used model PEO-PMMA blend systems prepared with various well-defined PEO architectures (linear, stars, hyper-branched and bottlebrushes) doped with lithium bis(trifluoromethanesulfonyl)-imide (LiTFSI), and investigated, for the first time, the role of macromolecular architecture of PEO on crystallization, segmental dynamics and ionic conductivity in the blends and electrolytes. The results suggest that room temperature miscibility of these polymers can be dramatically extended by using non-linear PEO in the blends instead of linear chains which crystallize above 35 wt. %. The broadband dielectric spectroscopy results revealed enhanced decoupling of PMMA and PEO segmental dynamics in compact branched architectures which helps to achieve faster segmental motion of star PEO in glassy PMMA. This manifests as nearly 3 fold higher ionic conductivity in these nonlinear blends compared to the conventional linear PEO-PMMA system. Overall, our results show that macromolecular architecture can be a new tool to decouple segmental dynamics and ion mobility to rationally design SPEs with improved performance.

INTRODUCTION

Polymers and their blends have been widely applied in various industries from aerospace and electric vehicles to consumer electronics and energy storage devices.¹⁻⁶ For most of these applications, lithium-ion batteries play a significant role, in which electrolytes are very critical for transporting positive lithium ions between electrodes.⁷ Liquid electrolytes that are currently in use are often flammable, volatile, toxic, and more prone to short circuit and leakage, leading to environmental and safety concerns.⁸⁻¹⁰ To overcome these disadvantages, solid polymer electrolytes (SPEs) have emerged as alternative systems for the fabrication of sustainable lithium-ion batteries.⁸⁻¹⁰ While SPEs provide decent mechanical stability,^{11, 12} deformability¹³ and biocompatibility,¹⁴ their low ionic conductivity at room temperature ($<10^{-5}$ S/cm)¹² compared to the liquid electrolytes ($\sim 10^{-2}$ S/cm)¹² remains as a major challenge for their commercial use.¹⁵

Linear poly(ethylene oxide) (PEO) has gained significant attention as SPE^{11, 15-17} due to its excellent characteristics including fast segmental dynamics as well as the ability of forming complexes with a wide range of different lithium salts. It is generally believed that ion conduction occurs in the amorphous phase where ion transport is coupled with segmental dynamics.^{11, 15, 16, 18-23} At room temperature, however, PEO is a semi-crystalline polymer with an ionic conductivity ranging between $10^{-6} - 10^{-8}$ S/cm,¹⁷ in which crystalline regions impede ion transport (see Figure 1a for scheme). The ionic conductivity increases up to 10^{-3} S/cm above its melting temperature ($T_m = 60^\circ\text{C}$),¹⁷ yet with severe reduction in mechanical strength, which limits its application in a solid-state battery. To overcome these drawbacks in relation to crystallization and mechanical stability, one method is to blend PEO with another polymer that can provide mechanical rigidity and eliminate crystallinity.^{11, 19-21} In this sense, a high glass transition temperature (T_g) polymer poly(methyl methacrylate) (PMMA) is commonly used (Figure 1b). Incorporation of PMMA significantly increased the mechanical

properties such as elastic modulus, young's modulus, as well as tensile strength for PEO/PMMA blend while it decreased the elongation at break.²⁴ The elimination of crystallinity requires thermodynamic miscibility of the polymers. Due to a slight attractive interaction between PEO and PMMA (χ ranges between -0.005 to -0.001),²⁵ the system is shown to be miscible up to 370 K.²⁶ Moreover, studies showed that crystallization of linear PEO in the blends is observed at concentrations exceeding 30% PEO.²⁷⁻²⁹ Also, the large difference between the T_g 's of the homopolymers ($\Delta T_g \sim 200$ K) causes significant slowdown of linear PEO segmental dynamics with the addition of PMMA.³⁰⁻³² As the lithium-ion transport occurs primarily in the amorphous phase, and is coupled with the segmental dynamics, increasing the amount of PEO without forming crystalline regions at higher concentrations and accelerating the segmental dynamics in the amorphous phase in the blend could further enhance the electrolyte performance. In this study, we show that both miscibility and dynamics of PEO in the blends with PMMA could be significantly enhanced when 'non-linear' PEO architectures, instead of commonly used linear chains, are employed.

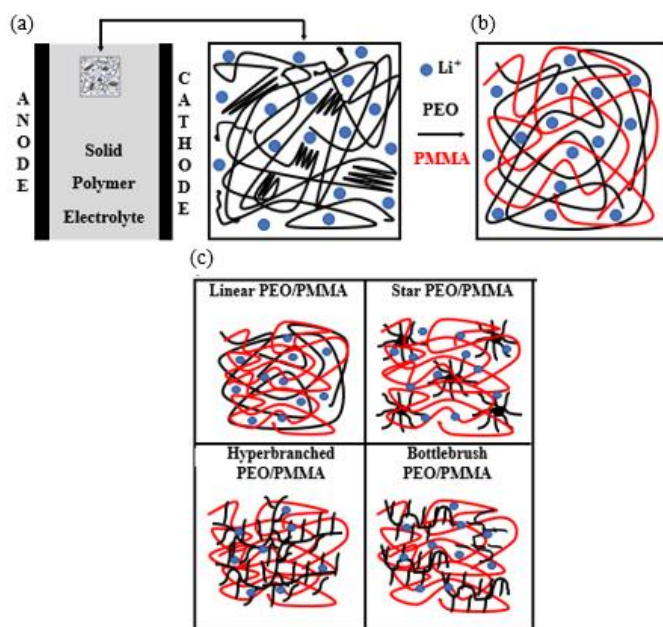


Figure 1. (a) Schematic depicting Li^+ ions in a semi-crystallized PEO electrolytes. (b) Sketch of an amorphous blend of Linear PEO/PMMA doped with Li^+ ions. (c) Schematic representation of linear and various non-linear topologies of PEO in blends with PMMA.

Several studies on the ‘neat’ PEO showed the effect of polymer topology on crystallization.^{15, 33-35} Zardalidis and co-workers³⁴ investigated the dependence of crystallization on molecular weight and architectures including linear and ring topologies and revealed that PEO with ring architecture exhibited lower crystallinity and apparent melting temperature compared to the linear analogue due to its more strained structure. In another work, Chen et al.³⁶ compared the degree of crystallization in linear and star PEO architectures (3-arms and 4-arms) and reported the crystallinity of star polymers was approximately 20% lower. Similarly, Coppola and co-workers studied crystallization of poly(ethylene oxide) star polymers of varying arm number and size and unveiled a slower crystallization kinetics of the stars compared to their linear analogues due to the high degree of branching with slowed

diffusivity.³³ Moreover, studies conducted by Yao et al.³⁵ and Lee et al.³⁷ showed that the crystallization of hyperbranched Poly(ethylene oxide) effectively decreased when compared to linear one because of the increased number of branching. These previous findings suggest that using non-linear PEO architectures can increase the fraction of amorphous PEO phase in which the ions are transported within SPEs, therefore, the PEO/PMMA blends have a significant potential to enhance the ionic conductivity when the nonlinear PEO architectures are used in the SPEs.

Also, the effect of free volume, which results from the free spaces between monomers along the (same or different) polymer chains,³⁸ on ionic conductivity was investigated by various studies in PEO-based SPEs.^{18, 22, 38, 39} The increase in free volume in the polymer matrix resulted in assisted ion migration, enhancing the ionic conductivity in these SPEs. Recent studies confirmed that the hampered crystallization of PEO due to the addition of nano-fillers or other polymers could increase the free volume.^{25, 40} Furthermore, it is known that increasing number of branches in the non-linear topologies resulted in a decrease in crystallization, increasing free volume.^{41, 42} The ion-migration within SPEs, known as hopping mechanism, is well established, in which the available free volume helps lithium ions to transport through hopping provided by the polymer segmental motions.^{18, 22, 38, 39} In this manner, Utpalla et al.³⁸ investigated the role of free volume and segmental dynamics on the ion conductivity of PEO based SPEs and found the increase in free volume with the addition of inorganic nano-fillers enhances the free volume fraction and decreases the crystallinity of pure PEO by increasing free available spaces between polymer chains, thus promotes the ionic conductivity. Similarly, Michael et al.⁴³ reported that the polymer chains leaning to coil up around nano-fillers added into PEO paved the way for the transportation of Li⁺ ions by providing the additional free volume as a result of decreasing crystallization. It is known that increasing number of branches in the non-linear topologies can result in an increase in free volume^{41, 42} due to enhanced

number of chain ends compared to the linear chains. Here, we take the advantage of enhanced free volume due to increased number of free end-groups in non-linear PEOs and suppressed crystallization arising from branching as well as PMMA addition to facilitate transportation of Li⁺ ions in PEO/PMMA blend electrolytes.

Very recently, the ionic conductivity in PEO/PMMA based solid polymer electrolytes (SPEs)¹¹ was investigated with star PMMA and linear PEO. Glynos and his co-workers revealed that the star PMMA in blends with linear PEO led to extremely fewer contacts between PEO and PMMA segments in comparison to the linear PMMA/PEO blends, giving rise to faster PEO segmental dynamics, thus resulting high ionic conductivity.¹¹ However, the key fundamental questions about the role of polymer topology on the polymer-polymer miscibility, the component segmental dynamics and correspondingly the ionic conductivity remain unanswered. In this work, we used various PEO topologies including linear, 4-arms, 8-arms, hyperbranched (6th generation, 6G) and bottlebrush, and dispersed in linear PMMA matrices to make a novel SPEs and investigated the role of polymer compactness, branching and interpenetration on phase behaviour, local dynamics, and ionic conductivity in polymer blend electrolytes.

EXPERIMENTAL METHODOLOGY

Materials

The PMMA homopolymer (MW~120kDa), linear PEO, hyperbranched (6th generation) PEO, and Lithium bis(trifluoromethane)sulfonamide, LiTFSI salt were purchased from Sigma-Aldrich. 4-arms and 8-arms star PEO were supplied by Creative PEGWorks. The bottlebrush PEO was synthesized in Center for Nanophase Materials Science (CNMS) of Oak Ridge National Laboratory. All polymers were used as received without modification. Table 1 displays their functionality, molar masses, and dispersities.

Table 1. Molecular characteristics of the PEO samples used in this study.

PEO architecture	Short name	Functionality /Arm number (f)	Total molecular weight (Mn) [kg/mol]	Arm molecular weight [kg/mol]	Dispersity (\mathcal{D})
Linear	L20	2	20	10	1.10
4-arms star	4F20	4	20	5	1.03
8-arms star	8F20	8	20	2.5	1.10
Hyperbranched	HB6G	6 th generation	35	NA	<1.5
Bottlebrush	BB	80	32	0.35	<1.2

Commented [E\$1]: @Kunlun, can we say this or another number here? Based on your experience.

Preparation of salt-free blend samples

Blends of various compositions of (PEO/PMMA) with topologies of linear (MW~20kDa), 4-arms star (MW~20kDa), 8-arms star (MW~20kDa), HB6G (MW~20kDa), bottle brush (MW~20kDa) PEO as well as pure PEO and PMMA were prepared by the solution casting technique. Polymers at desired ratios were first dissolved in chloroform at 30 mg/ml. Then, the solutions were stirred with a magnetic stirrer at room temperature for 6 hours. The solutions were then cast onto either glass petri dishes, and evaporated slowly for overnight at room temperature. Then, the dry films were transferred into a vacuum oven and annealed for 48 hours at 150°C to remove residual solvent. Finally, dielectric samples were prepared by hot pressing in a vacuum environment to form discs of 20 mm diameter and 200 μ thickness.

Preparation of Polymer Electrolytes

The desired amount of the lithium bis(trifluoromethane)sulfonamide, LiTFSI, was dissolved in acetonitrile, stirred for 48 hours. Then the disc samples were doped with (Li/EO=0.085) LiTFSI by solution uptake. The electrolytes were first dried at room

temperature for overnight in glovebox filled with Argon and annealed at 120°C in vacuum oven for 48 hours to ensure complete removal of the solvent.

Characterization

X-ray Diffraction (XRD): The XRD patterns of the pure PMMA, PEO and PEO/PMMA blends were recorded using the Bruker D2 Phaser – X-ray diffractometer with Cu K (α) source. The diffraction data were obtained at room temperature with the Bragg's angles (2θ) varying from 10 to 50 degrees.

Modulated differential Scanning Calorimetry (MDSC): The temperature modulated differential scanning calorimetry (MDSC) samples were prepared by putting ~8-10 mg of material in aluminium pans provided by TA Instruments. MDSC experiments of the pure PMMA, PEO and PEO/PMMA blends were carried out with a TA Instruments DSC25 instrument equipped with a liquid nitrogen cooling system. An aluminium pan was used as the reference. To get rid of the temperature history completely, all the samples were heated to 180 °C and waited there for 5 minutes. Samples were then quickly cooled down to -85°C at the rate of 20 °C/min. DSC scans were then collected during heating of the sample in modulated temperature mode at the ramp rate of 1 °C/min with a modulation amplitude $\pm 0.5^\circ\text{C}$ and period of 60 s.

Broadband Dielectric Spectroscopy (BDS): Dielectric relaxation spectra are obtained in the frequency range of $10^{-2} - 10^7$ Hz and the temperature range of 30°C to 90°C using an Alpha A analyzer (Novocontrol Co.). BDS measurements for linear and non-linear PEO/PMMA blends were performed with a temperature increase of 10°C and 30°C, respectively. At each temperature increase, the experiments were started once the temperature stability was reached within 0.05 K interval. After the experiments at high temperatures were over, we let the sample

cool to temperatures lower than 50°C, and only then the new sample was placed into the sample holder for the next measurements.

Electrochemical Impedance Spectroscopy (EIS): Impedance characterization was carried out using an Autolab Potentiostat Galvanostat PGSTAT (Metrohm, Netherlands) in two-electrode configuration for all PEO/PMMA blend electrolytes. This arrangement was used to investigate electrode properties in solid-state systems. The measurement frequency was varied between 1 Hz to 1 MHz. Each SPE blend disc was sandwiched between two stainless steel blocking electrodes under argon environment in a glove box located at Koç University Boron and Advanced Materials Application and Research Center (KUBAM) and sealed in MTI Split Cell to measure the complex impedance spectra. After waiting for the temperature stabilization of 0.1°C, the experiments were also carried out at various temperatures including 30, 60, and 90°C, respectively. The data was analysed to characterize real and imaginary impedances using the NOVA software.

RESULTS and DISCUSSION

Effect of PEO Architecture on the Crystallization in PEO/PMMA blends

We investigate the crystallization of neat PEO homopolymers and their blends with PMMA using XRD at room temperature. Figure 2 displays the concentration dependent intensity profiles for L20, 8F20 and BB PEO (see the results for 4F20 and HB6G in Figure S1). The peaks observed for the neat PEO samples at $2\theta=19^\circ$ (120-plane) and 23° (032-plane) confirmed the semi-crystalline nature of PEO^{11, 17, 44} and are the characteristic peaks of monoclinic lattice as the primary crystal structure.³⁴ Furthermore, regardless of the structural changes in PEO topologies, the positions of these peaks did not change, implying the primary monoclinic crystal structure as well as relative d-spacing of the predominant (120) and (032) planes are retained. Additionally, we found the degree of neat PEO crystallinity for different

architectures severely decreased with the number of branching. The representative crystallinity ratios are indicated by TableS1.

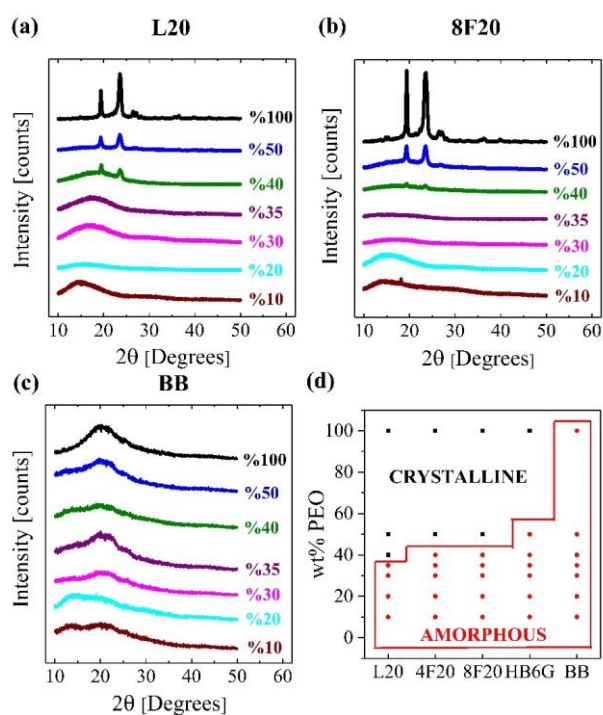


Figure 2. XRD results for (a) linear and non-linear topologies of PEO namely (b) 8-arms star and (c) bottle brush in blends with PMMA over a wide PEO composition (d) Crystallization phase map for various PEO architectures in blends with PMMA with respect to extensive PEO weight fraction

The addition of PMMA resulted in suppression of semi-crystalline nature of PEOs drastically, as also shown in previous studies in linear PEO/PMMA blends.^{27, 45-47} However, we show here that the degree of suppression changes differently based on the PEO topology. The linear PEO blended with PMMA crystallizes over 35wt% PEO in the blends whereas in the case of non-linear architectures, the amorphous blends containing higher amount of PEO

(up to 100%) can be formed. Specifically, in the case of 4-arms and 8-arms stars, the amorphous blends are obtained at 40% PEO concentrations, whereas this number can even reach up to 50% for the hyperbranched PEO. In the most extreme case, bottlebrush PEO (BB) was amorphous in its neat form and in blends with PMMA at all compositions, due to its densely grafted short side chains impeding formation of close-packed structure. Figure 2d displays the resulting phase diagram. The degree of crystallinity estimated using TMDSC are displayed in Table S1. All these results indicate that the crystallization in PEO/PMMA blends can be eliminated more effectively using PEO chains with high degree of branching. To the best of our knowledge, such a topology dependent crystallization in miscible blends is investigated for the first time in this work. As the ion transport is mediated by the amorphous phase of SPEs, this approach is of practical importance.

We chose 20% PEO concentration, where all blends are in the amorphous phase, to investigate the role of polymer architecture on dynamics, including glass transition, and segmental motion.

Effect of PEO Architecture on the Glass transition

We first investigate the effect of PEO topology on the glass transition in PEO/PMMA blends using modulated differential scanning calorimetry (TMDSC). Figure 3a shows the specific heat capacities (C_p 's) of neat PMMA and the blends with 20% PEO having different architectures. We found glass transition temperatures of neat PMMA and PEO with various architectures around 394 K and 220 K, respectively, in agreement with the previous reports (see Table S2 in Modulated differential scanning calorimetry (MDSC) results section for the details of T_g values for different PEO topologies).^{18, 19, 21, 30, 48} Since PMMA is the majority component, the heat flow in the blends is overwhelmed by PMMA signal. It is seen that the PMMA glass transition temperature in the blends shifts to lower values due to enhanced

mobility provided by low- T_g PEO segments. Even from the raw Cp data, it is evident that the transition is strongly architecture dependent.

Apart from the experimental techniques, several mathematical methods have been developed for estimating the glass transition temperature of mixtures from knowledge of the properties of the pure components. One of the most widely used equations for predicting glass transition temperatures of amorphous mixtures is the Fox equation given by the Eq.1:³¹

$$\frac{1}{T_g(\phi)} = \frac{\phi}{T_g^a} + \frac{1-\phi}{T_g^b} \quad (1)$$

where $T_g(\phi)$ and T_g^a as well as T_g^b are the glass transition temperature of the mixture and of the components, respectively, and ϕ is the weight fraction of component a. This model estimates one T_g , around 340 K for all blend systems, accounts for the glass transition temperature of the mixture using T_g values of the neat components and their weight fraction in a binary polymer blend. However, we observed two glass transition temperatures (T_g 's): one located at lower temperatures corresponding to the glass transition of the faster component, PEO, in the system and another one positioned at higher temperatures attributed to the slower component, PMMA. Although these polymers are miscible at macroscopic level, they are not homogenous at monomer level due to chain connectivity. Thus this forms a local heterogeneity, leading to concentration fluctuations in which some local regions spontaneously rich in one of the components in a binary polymer blend.³¹ This results in an average composition of the local environment around any chosen segment in comparison with the bulk composition is enriched in the same species, called as effective concentration.³¹ This results in two composition-dependent T_g 's (namely 'effective' T_g 's) in binary blends (see Modulated differential scanning calorimetry (MDSC) results section in the Supporting Information for the details of the Lodge-McLeish model).³¹ To highlight the effective T_g 's in the blends, the temperature derivative of the heat capacities are used (see Figure 3b). We fit a Gaussian $\propto \exp[-(T - T_g)^2 / (2(\Delta T_g)^2)]$

to find T_g and the entire peak widths at half-maximum height (ΔT_g) values more precisely.⁴⁹

The resulting effective T_g 's are given in Table 2 and displayed in Figure 3c.

Table 2. T_g and the transition width (ΔT_g) for all polymer blends, and its electrolytes containing 20wt% PEO with various PEO architectures.

Sample	BLEND				BLEND ELECTROLYTE	
	PEO		PMMA		PEO	PMMA
	T _{g,eff} , K	ΔT _g , K	T _{g,eff} , K	ΔT _g , K	T _{g,eff} , K	T _{g,eff} , K
L20	248.03	38.09	333.15	29.07	259.69	342.12
4F20	244.15	45.23	338.73	59.8	248.72	347.68
8F20	240.62	30.56	330	22.29	245.75	344.38
HB6G	260	32.48	360.5	36.51	266.15	371.57
BB	218.65	20	387.93	8.94	221.7	388.5

In addition, in comparison of T_{g-eff} values of PMMA in the blends with the T_g of neat PMMA, we found T_{g-eff} values were greatly shifted to the lower values due to increased mobility provided by low- T_g PEO segments. We also observed this transition was highly dependent on the PEO topology. It was seen the highest decrease in T_{g-eff} values of PMMA happened to be in blends with L20. The moderate increase in the number of branching in PEO architecture such as 4-arms and 8-arms stars slightly changed the degree of this decrease in T_{g-eff} values. Nevertheless, the shifts in T_{g-eff} of PMMA in blends with HB6G and BB, PEO architectures with the highest degree of branching, were significantly slowed down, leading the closest T_{g-eff} values in these blends to the T_g of neat PMMA. These findings are highly in accordance with our hypothesis that less interaction and interpenetration between PEO and PMMA was present in the case of non-linear PEO/PMMA blends.

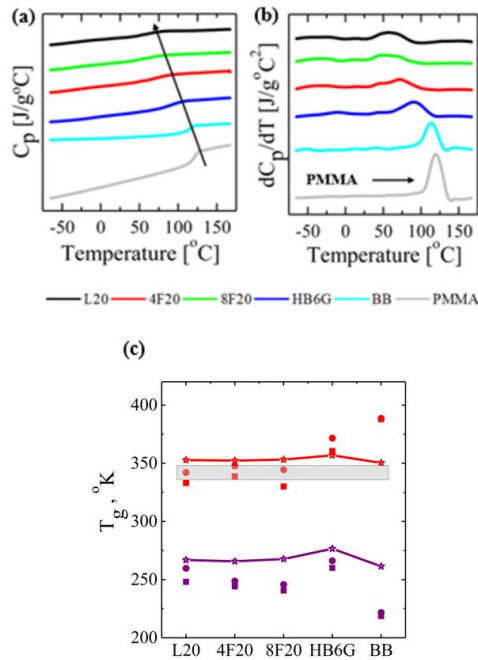


Figure 3. The dependence of the reversible heat flow (a) and its derivative (b) with respect to temperature for PEO with various topologies including linear, 4-arms, 8-arms, hyperbranched and bottle brush in blends with PMMA as well as neat PMMA. (c) The comparison of the experimental effective glass transition (T_{g-eff}) values for PEO and PMMA with the estimations obtained from DSC (Red and purple for filled squares and circles account for experimentally obtained values for T_{g-eff} of PMMA and PEO for blends and its electrolytes, respectively), Lodge-McLeish model (Red and purple stars with lines account for LM model estimated values for T_{g-eff} of PMMA and PEO for blends, respectively) and Fox model (Shaded region represent Fox model estimates for the blend T_g values)

We would like to emphasize that the Lodge-McLeish model has been tested by many studies with no emphasis on topological changes for these PEO/PMMA.^{32, 49-54} Recently, Lodge et al.^{32, 50} investigated the miscible blend system consisting of poly(ethylene oxide)

(PEO) and poly(methyl methacrylate) (PMMA) over the entire composition range using differential scanning calorimetry (DSC) to further comprehend the existence of two glass transition phenomenon. In their work, two distinct glass transition temperatures were clearly found in the mid-composition range.^{32, 50} In a different work, Colmenero and co-workers⁴⁹ examined the same polymer blend system through Modulated differential scanning calorimetry (MDSC) which depends on the changes in the heat capacity (C_p) of polymer samples and the presence of two glass transition temperatures within a certain composition for the PEO/PMMA blend was validated. Other significant studies applying the Lodge and McLeish model to PEO/PMMA blends have also confirmed the presence of two effective glass transition temperatures for the PMMA in PEO/PMMA blends.^{52, 53, 55} Our results are also consistent with these previous findings in terms of the existence of two effective glass transition temperatures. However, our experimentally obtained results through TMDSC quantitatively differed. In this context, the Figure 3c shows the comparisons between experimentally obtained T_{g-eff} values for PEO and PMMA and the estimations obtained using the prevalent mathematical models including Lodge and McLeish (self-concentration model) and Fox model. Regardless of the different topological changes in PEO topologies, both Lodge-McLeish and Fox Models were overestimating T_{g-eff} values for PEO, however they were generally better at predicting T_{g-eff} values for PMMA in all blends investigated. It appears that the theoretical self-concentration formulations which have been commonly used for linear polymer blends need to be modified when estimating the effective T_g 's in blends with non-linear topologies. Nevertheless, the research of this paper is not essentially interested in investigating the Lodge-McLeish model for non-linear polymer blends, which will be the subject of another work.

We finally analysed the PEO/PMMA/LTFSI based polymer electrolytes for the same PEO topologies including linear, 4-arms, 8-arms, hyperbranched and bottle brush. The reversible heat flow (a) and its derivative with respect to temperature (b) for

PEO/PMMA/LTFSI based polymer electrolytes with regards to various PEO topologies including linear, 4-arms, 8-arms, hyperbranched and bottle brush in blends are given in Figure S2 (see Modulated temperature differential scanning calorimetry results section in the Supporting Information for the details). Based on the derivative of the reversible heat flow with respect to temperature, estimated T_g effective values for PEO and PMMA using the derivative of the reversible heat flow with respect to temperature are shown in Table 2. We observed the architectural dependent transitions in the T_{g-eff} values of PMMA for all blends containing lithium salt (given in dots symbols in Figure 3c), thus the changes in the segmental dynamics associated with different polymer architectures and observed in salt-free samples in dielectric spectroscopy (discussed below) are effective also in the blend electrolytes.

Effect of PEO Architecture on the Segmental Dynamics and Ionic Conductivity

We next investigated the relaxation behaviour of the blends using broadband dielectric spectroscopy (BDS). Our aim here is to understand how different polymer topologies influence the segmental dynamics; thus, we use the salt-free blends at 20% PEO concentrations. Figure 4a and 4b display some representative dielectric spectra along with fits for neat PMMA and its 20wt% PEO blends at two different distinctive temperatures, specifically 328 K (lower than $T_{g, eff, PMMA}$) and 348 K (higher than $T_{g, eff, PMMA}$ for blends with linear and star PEOs). The dielectric loss spectra of PMMA and its 20wt% PEO blends (Figure 4a) at 328 K showed two processes, β -relaxation, and DC conductivity. However, at 348 K (Figure 4b) the α -relaxation of PMMA is also observed for L20, 4F20 and 8F20. Therefore, at 328 K, one Havriliak–Negami (HN) function was sufficient to define the PMMA dynamics for its neat form and respective blends with different PEOs whereas at 348 K, two Havriliak-Negami (HN) functions could define the relaxation involving β and α processes. In the frequency domain, the HN function is given as:⁵⁶

$$\varepsilon^* = \varepsilon_\infty + \frac{\Delta\varepsilon}{\left[1 + \left(\frac{i\omega}{\omega_0}\right)^a\right]^b} \quad (2)$$

where $\omega = 2\pi f$ is the angular frequency, and $\omega_0 = 2\pi f_0$ is a characteristic angular frequency related with the dielectric loss peak frequency (f_{max}). The relaxation strength $\Delta\varepsilon$ accounts for the difference between the real permittivity for low-frequency limiting value and that for high-frequency limiting value ε_∞ . The HN fitting parameter a is related to the broadness of the relaxation spectrum, while the parameter b describes its asymmetry, ($0 < a, b < 1$).

We found shape parameters for high and low frequency domains at 323 and 348 K is dependent on PEO topology. It is well established that the α -relaxation peak shape is correlated with segmental motions and essentially influenced by heterogeneity⁵⁷. It is seen that values for a parameter in the low frequency domain at 348 K increase with the increasing number of branching while b remains almost unchanged. These results suggest that the PMMA α -relaxation spectra of the linear PEO/PMMA blend is broader than the non-linear ones. Furthermore, the values for the low frequency domain at 348 K are hardly affected by PEO topology whereas b values decrease in the case of non-linear blends, indicating that β relaxation spectra being more asymmetric as degree of branching become higher. Also, a parameter for 323 K increase with decreasing b values as more compact PEO was employed. Smaller a and higher b values indicate the spectra for the β relaxation becomes narrower and less symmetric when non-linear PEO/PMMA blends are employed, suggesting more heterogeneous dynamics. The shape parameters (a, b) resulting from HN fitting for high frequency and low frequency relaxation dynamics at 323 and 348 K are summarized in Table S6 (see Broadband Dielectric Spectroscopic Analysis (BDS) results section in the Supporting Information for the details).

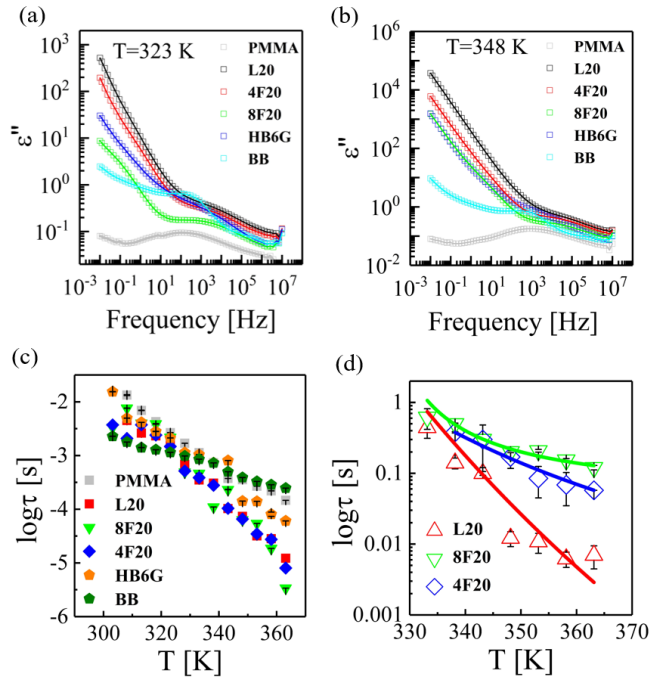


Figure 4. The frequency dependence of the dielectric relaxation data at 323 K and 348 K (b) along with HN fits in linear and non-linear PEO/PMMA blends. The temperature dependence of β relaxation (c) for neat PMMA, linear, 4-arms, 8-arms, hyperbranched, and bottle brush PEO architectures, and α relaxation dynamics (d) for PMMA in blends with various PEO architectures including only linear, 4-arms, and 8-arms.

Figure 4c and 4d show the relaxation times as a function of temperature for β and α processes of PMMA in its neat form and its 20% wt PEO blends, respectively. For all samples within the temperature of investigation, we observed the β relaxation process following the Arrhenius behaviour expressed as:^{56, 58-61}

$$\tau_{\beta} = \tau_0 \exp\left(\frac{E_{\beta}}{RT}\right) \quad (3)$$

where τ_0 is the reference time, E_β is the active energy of relaxation, and R is the gas constant number ($8.314 \frac{J}{mol K}$). Based on these Arrhenius fits, the activation energy (E_β) and τ_0 for pure PMMA were calculated as 7.55 kJ/mol and $1.86 * 10^{-15}$ s, which is in very good agreement with the reported results.^{56, 58, 60, 61} All the results regarding the activation energy (E_β) and reference time (τ_0) for L20, 4F20, 8F20, HB6G, and BB PEO architectures in the blends are summarized in Table S3 (see Broadband Dielectric Spectroscopic Analysis (BDS) results section in the Supporting Information for the details). Furthermore, it was seen that α relaxation for PMMA dynamics in all blends with PEO decreased with temperature following a Vogel-Tamman-Fulcher VFT type of behaviour given by:⁵⁵

$$\tau_\alpha = \tau_\infty \exp\left(\frac{B}{T-T_v}\right) \quad (4)$$

where τ_∞ accounts for the extrapolated relaxation time at infinite temperatures, B, and T_v are VFT constants for a given component in a particular blend. VFT parameters for 20wt% blends of L20, 4F20, and 8F20 are given by Table S4 (see Broadband Dielectric Spectroscopic Analysis (BDS) results section in the Supporting Information for the details).

We specifically observed PMMA segmental dynamics in blends with L20 to be faster due to enhanced mobility provided by low T_g -PEO, resulting declines in its relaxation times. More strikingly, compared to the linear blend, it was found that the α relaxation of PMMA is slower in the case of non-linear PEO architectures, including 4-arms and 8- arms stars, (see Figure 4d). As the compactness increases with branching, the interpenetrability of PMMA and PEO decreases with increasing number of arms; thus PMMA in the presence of 8 arms-star PEO exhibit slower segmental dynamics. Using the argument, the influence of PMMA on the slowing down of PEO segmental motion is also less in the case of non-linear topologies. Therefore, the PEO segmental dynamics is expected to be faster in the non-linear

PEO/PMMA blends when compared to the linear counterpart. This suggests that higher ionic conductivity in non-linear polymer blend electrolytes can be realized.

To test this hypothesis, we prepared PEO/PMMA blend electrolytes containing 50 wt.% PEO and LiTFSI at $[Li^+]/[EO] = 0.085$ ratio.

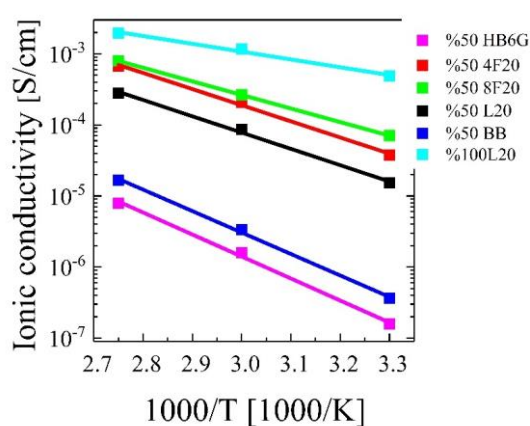


Figure 5. The ionic conductivity measurements with corresponding Arrhenius fit lines for the solid polymer blend electrolytes prepared using neat PEO and 50wt% PEO in blends with PMMA at various temperatures including 30°C, 60°C, and 90°C, respectively for different PEO architectures.

Figure 5 illustrates the ionic conductivities of the electrolytes at 30°C, 60°C, and 90°C obtained from electrochemical impedance spectroscopy (see Figure S5 for the Nyquist plot for the calculation details of the ionic conductivity). We have also prepared an electrolyte with the linear PEO only to compare with the blends. The neat PEO/LiTFSI resulted in an ionic conductivity $\sim 10^{-3}$ S/cm at 60 °C, which is in agreement with previously reported results.^{11, 15, 16, 38, 62} In the case of the blend electrolytes, the ionic conductivity for blend with the linear PEO decreased about an order of magnitude, as expected due to its slower segment dynamics in presence of PMMA.¹¹ More importantly, the ionic conductivity in the blends is strongly

architecture dependent. The electrolytes with 4-arms and 8-arms stars significantly enhanced the conductivity, specifically 2.5x for 4-arms and 3x for 8-arms at 60 °C, mainly due to faster PEO segmental dynamics compared to the linear one as predicted from BDS measurements. However, blends electrolytes with the bottlebrush and hyperbranched PEO resulted in dramatic decrease in conductivity (25x for BB and for 55x HB6G compared to L20 at 60 °C). This is likely due to high fraction of hydroxyl-terminated end groups which interact with the salt ions by forming a transient cross-linking and limit its mobility as well as lithium migration. Thus, further increase in the number of branching in PEO architectures may dramatically reduce the positive effects provided by faster PEO segmental dynamics, increasing free volume and lowered degree of crystallization provided by non-linear PEO topologies in the blends, and can even decrease the lithium mobility as seen here for the extreme cases of hyperbranched and bottlebrush PEO. The activation energies obtained from the Arrhenius plots in Figure 5 suggests that the lithium-ion transportation in the SPEs is due to the ion-hopping mechanism⁶³, regardless of the PEO topology. However, the estimated activation energies are strongly architecture dependent (see Table S5 for activation energies for SPEs with various topologies). The blend electrolyte with linear PEO has activation energy 0.47 eV (comparable to the previously reported values ~0.5 eV⁶⁴) whereas it decreases to 0.45 and 0.38 for 4-arms and 8-arms star PEO which display higher ionic conductivity. On the other hand, the activation energies estimated for the electrolytes with hyperbranched and bottlebrush PEO increase to \approx 0.62 eV, supporting the argument that increased hydroxyl-Li⁺ interaction in these highly branched structures impede the ion mobility.

Finally, we would like to note that we used the same [Li⁺]/[EO] ratio of 0.085 for all blend electrolytes as the conductivity peaks at this ratio for PEO. However, this might also be architecture dependent and the phase behaviour or PEO-LiTFSI need to be further investigated with non-linear polymer architectures to further improve the performance of the homopolymer

and blend based SPEs. This is currently under investigation and will be discussed in another article.

CONCLUSIONS

In conclusion, we studied the effects of chain topology on miscibility, glass transition, segmental dynamics, and ionic conductivity for the poly(ethylene oxide)-poly(methyl methacrylate) doped with lithium bis(trifluoromethane-sulfonyl)-imide (LiTFSI) blend systems. Various well-defined PEO architectures, specifically linear, stars, hyper-branched and bottlebrushes, and compositions were investigated. Our XRD results reveal that room temperature miscibility of these polymers can be significantly extended by using non-linear architectures of PEO relative to the linear blend which crystallizes above 35% of PEO concentration. In the amorphous PEO/PMMA blends including 20%PEO, temperature modulated DSC results suggest tunability of the effective glass transition temperatures of both PEO and PMMA components with polymer architecture. Additionally, our broadband dielectric spectroscopy measurements show strong dependence of PMMA segmental dynamics on the PEO topologies. Increasing number of branches in the PEO helps to maintain its fast segmental dynamics even in the blends with glassy PMMA due to less interaction sites and interpenetration of PMMA into compact and nonlinear PEO. This manifests as 2.5- and 3-fold higher ionic conductivity (with respect to the linear PEO at the same molar mass) in blends with 4-arms and 8-arms stars, respectively. Interestingly, the electrolytes with hyperbranched and bottlebrush PEO displayed more than an order of magnitude decrease in conductivity, possibly due to lithium complexation with the hydroxyl terminated end groups. Overall, our results show that the macromolecular architecture can be an effective tool for improving ionic conductivity in polymer blend based solid electrolytes.

ASSOCIATED CONTENT

Supporting Information. The Supporting Information is available free of charge at:

X-ray Diffraction (XRD), Modulated differential Scanning Calorimetry (MDSC), and Electrochemical Impedance Spectroscopy (EIS) results: (PDF)

AUTHOR INFORMATION

Corresponding Author

*Erkan Senses – Chemical and Biological Engineering, Koc University, Sariyer, Istanbul 34450, Turkey; <https://orcid.org/0000-0003-2593-1146>, Email: esenses@ku.edu.tr

Author Contributions

All authors have given approval to the final version of the manuscript.

Notes

The authors declare no competing financial interest.

ACKNOWLEDGMENT

E.S. acknowledges support through Koç University SEED Research Grant (SF.00078). We thank Koç University Boron and Advanced Materials Application and Research Center (KUBAM) for their help with electrolyte sample preparation. We also acknowledge Koç University Surface Science and Technology Center (KUYTAM) and Dr. Hadi Jahangiri for their assistance on the XRD measurements. We are grateful to The Center for Nanophase Materials Sciences (CNMS) at Oak Ridge National Laboratory (ORNL) for providing the bottlebrush sample.

REFERENCES

1. Habib, A. K. M. A.; Hasan, M. K.; Mahmud, M.; Motakabber, S. M. A.; Ibrahimya, M. I.; Islam, S., A review: Energy storage system and balancing circuits for electric vehicle application. *IET Power Electronics* **2021**, *14* (1), 1-13.
2. SubramanianDr., C., An appraisal on intelligent and smart systems. *AIP Conference Proceedings* **2021**, *2316* (1), 020003.
3. Rodriguez, R. D.; Shchadenko, S.; Murastov, G.; Lipovka, A.; Fatkullin, M.; Petrov, I.; Tran, T.-H.; Khalelov, A.; Saqib, M.; Villa, N. E.; Bogoslovskiy, V.; Wang, Y.; Hu, C.-G.; Zinovyev, A.; Sheng, W.; Chen, J.-J.; Amin, I.; Sheremet, E., Ultra-Robust Flexible Electronics by Laser-Driven Polymer-Nanomaterials Integration. *Advanced Functional Materials* **2021**, *31* (17), 2008818.
4. Wang, J.; Li, S.; Zhao, Q.; Song, C.; Xue, Z., Structure Code for Advanced Polymer Electrolyte in Lithium-Ion Batteries. *Advanced Functional Materials* **2021**, *31* (12), 2008208.
5. Xia, Y.; He, Y.; Zhang, F.; Liu, Y.; Leng, J., A Review of Shape Memory Polymers and Composites: Mechanisms, Materials, and Applications. *Advanced Materials* **2021**, *33* (6), 2000713.
6. Rinaldi, M.; Cecchini, F.; Pigliaru, L.; Ghidini, T.; Lumaca, F.; Nanni, F., Additive Manufacturing of Polyether Ether Ketone (PEEK) for Space Applications: A Nanosat Polymeric Structure. *Polymers* **2021**, *13* (1), 11.
7. Schaefer, J. L.; Lu, Y.; Moganty, S. S.; Agarwal, P.; Jayaprakash, N.; Archer, L. A., Electrolytes for high-energy lithium batteries. *Applied Nanoscience* **2012**, *2* (2), 91-109.
8. Choo, Y.; Halat, D. M.; Villaluenga, I.; Timachova, K.; Balsara, N. P., Diffusion and migration in polymer electrolytes. *Progress in Polymer Science* **2020**, *103*, 101220.
9. Armand, M.; Axmann, P.; Bresser, D.; Copley, M.; Edström, K.; Ekberg, C.; Guyomard, D.; Lestriez, B.; Novák, P.; Petranikova, M.; Porcher, W.; Trabesinger, S.;

- Wohlfahrt-Mehrens, M.; Zhang, H., Lithium-ion batteries – Current state of the art and anticipated developments. *Journal of Power Sources* **2020**, *479*, 228708.
10. Zhou, D.; Shanmukaraj, D.; Tkacheva, A.; Armand, M.; Wang, G., Polymer Electrolytes for Lithium-Based Batteries: Advances and Prospects. *Chem* **2019**, *5* (9), 2326-2352.
 11. Glynos, E.; Petropoulou, P.; Mygiakis, E.; Nega, A. D.; Pan, W.; Papoutsakis, L.; Giannelis, E. P.; Sakellariou, G.; Anastasiadis, S. H., Leveraging Molecular Architecture To Design New, All-Polymer Solid Electrolytes with Simultaneous Enhancement in Modulus and Ionic Conductivity. *Macromolecules* **2018**, *51* (7), 2542-2550.
 12. Chen, R.; Qu, W.; Guo, X.; Li, L.; Wu, F., The pursuit of solid-state electrolytes for lithium batteries: from comprehensive insight to emerging horizons. *Materials Horizons* **2016**, *3* (6), 487-516.
 13. Kim, S.-H.; Choi, K.-H.; Cho, S.-J.; Park, J.-S.; Cho, K. Y.; Lee, C. K.; Lee, S. B.; Shim, J. K.; Lee, S.-Y., A shape-deformable and thermally stable solid-state electrolyte based on a plastic crystal composite polymer electrolyte for flexible/safer lithium-ion batteries. *Journal of Materials Chemistry A* **2014**, *2* (28), 10854-10861.
 14. Lin, Y.; Cheng, Y.; Li, J.; Miller, J. D.; Liu, J.; Wang, X., Biocompatible and biodegradable solid polymer electrolytes for high voltage and high temperature lithium batteries. *RSC Advances* **2017**, *7* (40), 24856-24863.
 15. Stolwijk, N. A.; Wiencierz, M.; Heddier, C.; Kösters, J., What Can We Learn from Ionic Conductivity Measurements in Polymer Electrolytes? A Case Study on Poly(ethylene oxide) (PEO)-NaI and PEO-LiTFSI. *The Journal of Physical Chemistry B* **2012**, *116* (10), 3065-3074.
 16. Mongcopa, K. I. S.; Tyagi, M.; Mailoa, J. P.; Samsonidze, G.; Kozinsky, B.; Mullin, S. A.; Gribble, D. A.; Watanabe, H.; Balsara, N. P., Relationship between

Segmental Dynamics Measured by Quasi-Elastic Neutron Scattering and Conductivity in Polymer Electrolytes. *ACS Macro Letters* **2018**, 7 (4), 504-508.

17. Glynos, E.; Pantazidis, C.; Sakellariou, G., Designing All-Polymer Nanostructured Solid Electrolytes: Advances and Prospects. *ACS Omega* **2020**, 5 (6), 2531-2540.

18. Devaux, D.; Bouchet, R.; Glé, D.; Denoyel, R., Mechanism of ion transport in PEO/LiTFSI complexes: Effect of temperature, molecular weight and end groups. *Solid State Ionics* **2012**, 227, 119-127.

19. Feng, J.; Wang, L.; Chen, Y.; Wang, P.; Zhang, H.; He, X., PEO based polymer-ceramic hybrid solid electrolytes: a review. *Nano Convergence* **2021**, 8 (1), 2.

20. Zhao, Y.; Bai, Y.; Li, W.; An, M.; Bai, Y.; Chen, G., Design Strategies for Polymer Electrolytes with Ether and Carbonate Groups for Solid-State Lithium Metal Batteries. *Chemistry of Materials* **2020**, 32 (16), 6811-6830.

21. Jokhakar, D. A.; Puthusseri, D.; Manikandan, P.; Li, Z.; Moon, J.; Weng, H.-J.; Pol, V. G., All-solid-state Li-metal batteries: role of blending PTFE with PEO and LiTFSI salt as a composite electrolyte with enhanced thermal stability. *Sustainable Energy & Fuels* **2020**, 4 (5), 2229-2235.

22. Bresser, D.; Lyonard, S.; Iojoiu, C.; Picard, L.; Passerini, S., Decoupling segmental relaxation and ionic conductivity for lithium-ion polymer electrolytes. *Molecular Systems Design & Engineering* **2019**, 4 (4), 779-792.

23. Jr., D. T. H.; Balsara, N. P., Polymer Electrolytes. *Annual Review of Materials Research* **2013**, 43 (1), 503-525.

24. Zainal, N. F. A.; Lai, S. A.; Chan, C. H., Melt Rheological Behavior and Morphology of Poly(ethylene oxide)/Natural Rubber-graft-Poly(methyl methacrylate) Blends. *Polymers (Basel)* **2020**, 12 (3).

25. Ito, H.; Russell, T. P.; Wignall, G. D., Interactions in mixtures of poly(ethylene oxide) and poly(methyl methacrylate). *Macromolecules* **1987**, *20* (9), 2213-2220.
26. Cimmino, S.; Martuscelli, E.; Silvestre, C., Miscibility prediction based on the corresponding states theory: poly(ethylene oxide)/atactic poly(methyl methacrylate) system. *Polymer* **1989**, *30* (3), 393-398.
27. Madalena, D., Anabela, C. F., Joa, F. M., Natalia, T. C., and Rui C. S., Relaxation Studies in PEO/PMMA Blends. *Macromolecules* **2000**, *33* (3), 1002-1011.
28. Xing Jin, S. Z., and James Runt, Broadband Dielectric Investigation of Amorphous Poly(methylmethacrylate)/Poly(ethylene oxide) Blends. *Macromolecules* **2004**, *37* (21), 8110-8115.
29. Dionísio, M.; Fernandes, A. C.; Mano, J. F.; Correia, N. T.; Sousa, R. C., Relaxation Studies in PEO/PMMA Blends. *Macromolecules* **2000**, *33* (3), 1002-1011.
30. Senses, E.; Tyagi, M.; Pasco, M.; Faraone, A., Dynamics of Architecturally Engineered All-Polymer Nanocomposites. *ACS Nano* **2018**, *12* (11), 10807-10816.
31. McLeish, T. P. L. a. T. C. B., Self-Concentrations and Effective Glass Transition Temperatures in Polymer Blends. *Macromolecules* **2000**, *33* (14), 5278-5284.
32. Lodge, T. P.; Wood, E. R.; Haley, J. C., Two calorimetric glass transitions do not necessarily indicate immiscibility: The case of PEO/PMMA. *Journal of Polymer Science Part B: Polymer Physics* **2006**, *44* (4), 756-763.
33. Coppola, S.; Grizzuti, N.; Floudas, G.; Vlassopoulos, D., Viscoelasticity and crystallization of poly(ethylene oxide) star polymers of varying arm number and size. *Journal of Rheology* **2007**, *51* (5), 1007-1025.
34. Zardalidis, G.; Mars, J.; Allgaier, J.; Mezger, M.; Richter, D.; Floudas, G., Influence of chain topology on polymer crystallization: poly(ethylene oxide) (PEO) rings vs. linear chains. *Soft Matter* **2016**, *12* (39), 8124-8134.

35. Yao, Y.; Suzuki, Y.; Seiwert, J.; Steinhart, M.; Frey, H.; Butt, H.-J.; Floudas, G., Capillary Imbibition, Crystallization, and Local Dynamics of Hyperbranched Poly(ethylene oxide) Confined to Nanoporous Alumina. *Macromolecules* **2017**, *50* (21), 8755-8764.
36. Chen, E.-Q.; Lee, S.-W.; Zhang, A.; Moon, B.-S.; Mann, I.; Harris, F. W.; Cheng, S. Z. D.; Hsiao, B. S.; Yeh, F.; von Meerwall, E. D.; Grubb, D. T., Isothermal Thickening and Thinning Processes in Low-Molecular-Weight Poly(ethylene oxide) Fractions Crystallized from the Melt. 8. Molecular Shape Dependence. Volume 32, Number 15, July 27, 1999, pp 4784–4793. *Macromolecules* **1999**, *32* (15), 5174-5174.
37. Lee, S.-I.; Schömer, M.; Peng, H.; Page, K. A.; Wilms, D.; Frey, H.; Soles, C. L.; Yoon, D. Y., Correlations between Ion Conductivity and Polymer Dynamics in Hyperbranched Poly(ethylene oxide) Electrolytes for Lithium-Ion Batteries. *Chemistry of Materials* **2011**, *23* (11), 2685-2688.
38. Utpalla, P.; Sharma, S. K.; Deshpande, S. K.; Bahadur, J.; Sen, D.; Sahu, M.; Pujari, P. K., Role of free volumes and segmental dynamics on ion conductivity of PEO/LiTFSI solid polymer electrolytes filled with SiO₂ nanoparticles: a positron annihilation and broadband dielectric spectroscopy study. *Physical Chemistry Chemical Physics* **2021**, *23* (14), 8585-8597.
39. SHOJAATALHOSSEINI, M. Conductivity and Relaxation in Polymer Based Solid Electrolyte. Master Thesis, Chalmers University of Technology, Gothenburg, Sweden, 2016.
40. Homann, G.; Stolz, L.; Nair, J.; Laskovic, I. C.; Winter, M.; Kasnatscheew, J., Poly(Ethylene Oxide)-based Electrolyte for Solid-State-Lithium-Batteries with High Voltage Positive Electrodes: Evaluating the Role of Electrolyte Oxidation in Rapid Cell Failure. *Scientific Reports* **2020**, *10* (1), 4390.
41. Chremos, A.; Douglas, J. F., Communication: When does a branched polymer become a particle? *The Journal of Chemical Physics* **2015**, *143* (11), 111104.

42. Chremos, A.; Glynos, E.; Green, P. F., Structure and dynamical intra-molecular heterogeneity of star polymer melts above glass transition temperature. *The Journal of Chemical Physics* **2015**, *142* (4), 044901.
43. Michael, M. S.; Jacob, M. M. E.; Prabakaran, S. R. S.; Radhakrishna, S., Enhanced lithium ion transport in PEO-based solid polymer electrolytes employing a novel class of plasticizers. *Solid State Ionics* **1997**, *98* (3), 167-174.
44. Xue, Z.; He, D.; Xie, X., Poly(ethylene oxide)-based electrolytes for lithium-ion batteries. *Journal of Materials Chemistry A* **2015**, *3* (38), 19218-19253.
45. G. C. Alfonso and T. P. R., Kinetics of Crystallization in Semicrystalline/ Amorphous Polymer Mixtures. *Macromolecules* **1986**, *19* (4), 1143-1152.
46. Alfonso, G. C.; Russell, T. P., Crystallization and Melting Studies on Poly (Ethylene Oxide)/Poly (Methyl Methacrylate) Mixtures. In *Integration of Fundamental Polymer Science and Technology*, Kleintjens, L. A.; Lemstra, P. J., Eds. Springer Netherlands: Dordrecht, 1986; pp 132-137.
47. Yap, Y. L.; You, A. H.; Teo, L. L., Preparation and characterization studies of PMMA–PEO-blend solid polymer electrolytes with SiO₂ filler and plasticizer for lithium ion battery. *Ionics* **2019**, *25* (7), 3087-3098.
48. Straka, J.; Schmidt, P.; Dybal, J.; Schneider, B.; Spěváček, J., Blends of poly(ethylene oxide)/poly(methyl methacrylate). An i.r. and n.m.r. study. *Polymer* **1995**, *36* (6), 1147-1155.
49. Bhowmik, D.; Pomposo, J. A.; Juranyi, F.; García Sakai, V.; Zamponi, M.; Arbe, A.; Colmenero, J., Investigation of a Nanocomposite of 75 wt % Poly(methyl methacrylate) Nanoparticles with 25 wt % Poly(ethylene oxide) Linear Chains: A Quasielastic Neutron Scattering, Calorimetric, and WAXS Study. *Macromolecules* **2014**, *47* (9), 3005-3016.

50. Gaikwad, A. N.; Wood, E. R.; Ngai, T.; Lodge, T. P., Two Calorimetric Glass Transitions in Miscible Blends Containing Poly(ethylene oxide). *Macromolecules* **2008**, *41* (7), 2502-2508.
51. García Sakai, V.; Maranas, J. K.; Peral, I.; Copley, J. R. D., Dynamics of PEO in Blends with PMMA: Study of the Effects of Blend Composition via Quasi-Elastic Neutron Scattering. *Macromolecules* **2008**, *41* (10), 3701-3710.
52. He, Y.; Lutz, T. R.; Ediger, M. D., Segmental and terminal dynamics in miscible polymer mixtures: Tests of the Lodge–McLeish model. *The Journal of Chemical Physics* **2003**, *119* (18), 9956-9965.
53. Mpoukouvalas, K.; Floudas, G., Effect of Pressure on the Dynamic Heterogeneity in Miscible Blends of Poly(methyl methacrylate) with Poly(ethylene oxide). *Macromolecules* **2008**, *41* (4), 1552-1559.
54. Kalogeras, I. M.; Brostow, W., Glass transition temperatures in binary polymer blends. *Journal of Polymer Science Part B: Polymer Physics* **2009**, *47* (1), 80-95.
55. Lutz, T. R.; He, Y.; Ediger, M. D.; Cao, H.; Lin, G.; Jones, A. A., Rapid Poly(ethylene oxide) Segmental Dynamics in Blends with Poly(methyl methacrylate). *Macromolecules* **2003**, *36* (5), 1724-1730.
56. Bergman, R.; Alvarez, F.; Alegría, A.; Colmenero, J., The merging of the dielectric α - and β -relaxations in poly-(methyl methacrylate). *The Journal of Chemical Physics* **1998**, *109* (17), 7546-7555.
57. Lin, Y.; Tan, Y.; Qiu, B.; Cheng, J.; Wang, W.; Shangguan, Y.; Zheng, Q., Casting solvent effects on molecular dynamics of weak dynamic asymmetry polymer blend films via broadband dielectric spectroscopy. *Journal of Membrane Science* **2013**, *439*, 20-27.

58. Hirota, S.-I.; Tominaga, Y.; Asai, S.; Sumita, M., Dielectric relaxation behavior of poly(methyl methacrylate) under high-pressure carbon dioxide. *Journal of Polymer Science Part B: Polymer Physics* **2005**, *43* (21), 2951-2962.
59. Jin, X.; Zhang, S.; Runt, J., Broadband Dielectric Investigation of Amorphous Poly(methyl methacrylate)/Poly(ethylene oxide) Blends. *Macromolecules* **2004**, *37* (21), 8110-8115.
60. Seki, Y.; Kita, R.; Shinyashiki, N.; Yagihara, S.; Yoneyama, M., Molecular dynamics of poly(methyl methacrylate) determined by dielectric relaxation spectroscopy. *AIP Conference Proceedings* **2013**, *1518* (1), 466-469.
61. Sakai, V. G.; Chen, C.; Maranas, J. K.; Chowdhuri, Z., Effect of Blending with Poly(ethylene oxide) on the Dynamics of Poly(methyl methacrylate): A Quasi-Elastic Neutron Scattering Approach. *Macromolecules* **2004**, *37* (26), 9975-9983.
62. Lin, D.; Liu, W.; Liu, Y.; Lee, H. R.; Hsu, P.-C.; Liu, K.; Cui, Y., High Ionic Conductivity of Composite Solid Polymer Electrolyte via In Situ Synthesis of Monodispersed SiO₂ Nanospheres in Poly(ethylene oxide). *Nano Letters* **2016**, *16* (1), 459-465.
63. Ahmed, H. T.; Abdullah, O. G., Structural and ionic conductivity characterization of PEO:MC-NH₄I proton-conducting polymer blend electrolytes based films. *Results in Physics* **2020**, *16*, 102861.
64. Unge, M.; Gudla, H.; Zhang, C.; Brandell, D., Electronic conductivity of polymer electrolytes: electronic charge transport properties of LiTFSI-doped PEO. *Physical Chemistry Chemical Physics* **2020**, *22* (15), 7680-7684.

For Table of Contents Only

